Atmos. Chem. Phys., 3, 1131–1145, 2003
www.atmos-chem-phys.org/acp/3/1131/

Atmospheric Chemistry and Physics

The rate of water vapor evaporation from ice substrates in the presence of HCl and HBr: implications for the lifetime of atmospheric ice particles

C. Delval, B. Fluckiger, and M. J. Rossi

Laboratory of Air and Soil Pollution Studies (LPAS), Swiss Federal Institute of Technology (EPFL), CH-1015 Lausanne, Switzerland

Received: 4 March 2003 – Published in Atmos. Chem. Phys. Discuss.: 9 May 2003
Revised: 10 July 2003 – Accepted: 24 July 2003 – Published: 21 August 2003

Abstract. Using a multidiagnostic approach the rate R_{ev} [molec cm^{-3} s^{-1}] or flux J_{ev} [molec cm^{-2} s^{-1}] of evaporation of H_2O and its corresponding rate constant for condensation, k_{cond} [s^{-1}], on a 1 μm thick ice film have been studied in the temperature range 190 to 240 K as well as in the presence of small amounts of HCl and HBr that left the vapor pressure of H_2O on ice unchanged. The resulting Arrhenius expressions for pure ice are $J_{ev} = 1.6 \cdot 10^{28\pm1} \cdot \exp\left(\frac{-10.3\pm1.2}{RT}\right)$ [molec cm^{-2} s^{-1}], $k_{cond} = 1.7 \cdot 10^{-2\pm1} \cdot \exp\left(\frac{+1.6\pm1.5}{RT}\right)$ [s^{-1}], in the presence of a HCl mole fraction in the range $3.2 \cdot 10^{-5} - 6.4 \cdot 10^{-3}$: $J_{ev} = 6.4 \cdot 10^{26\pm1} \cdot \exp\left(\frac{-9.7\pm1.2}{RT}\right)$ [molec cm^{-2} s^{-1}], $k_{cond} = 2.8 \cdot 10^{-3\pm1} \cdot \exp\left(\frac{+1.5\pm1.6}{RT}\right)$ [s^{-1}], and a HBr mole fraction smaller than $6.4 \cdot 10^{-3}$: $J_{ev} = 7.4 \cdot 10^{25\pm1} \cdot \exp\left(\frac{-9.1\pm1.2}{RT}\right)$ [molec cm^{-2} s^{-1}], $k_{cond} = 7.1 \cdot 10^{-5\pm1} \cdot \exp\left(\frac{+2.6\pm1.5}{RT}\right)$ [s^{-1}]. The small negative activation energy for H_2O condensation on ice points to a precursor mechanism. The corresponding enthalpy of sublimation is $\Delta H_{subl} = E_{ev} - E_{cond} = 11.9 \pm 2.7$ kcal mol^{-1}, $\Delta H_{subl} = 11.2 \pm 2.8$ kcal mol^{-1}, and $\Delta H_{subl} = 11.7 \pm 2.8$ kcal mol^{-1} whose values are identical within experimental uncertainty to the accepted literature value of 12.3 kcal mol^{-1}. Interferometric data at 633 nm and FTIR absorption spectra in transmission support the kinetic results. The data are consistent with a significant lifetime enhancement for HCl- and HBr-contaminated ice particles by a factor of 3–6 and 10–20, respectively, for submonolayer coverages of HX once the fraction of the ice not contaminated by HX has evaporated.

Correspondence to: M. J. Rossi (michel.rossi@epfl.ch)

1 Introduction

Heterogeneous reactions occurring on the surface of polar stratospheric clouds (PSC's) are known to play an important role in controlling the abundance of O_3 in the polar stratosphere by converting hydrogen halide reservoir species HX (X = Br,Cl) into photolytically active halogens (Solomon et al., 1986; Tolbert et al., 1987; Wennberg et al., 1997; WMO Report, 2002). In addition, recent studies indicate that Cirrus cloud ice particles near the tropopause may act as substrates for heterogeneous reactions akin to PSC's with a similarly high efficiency (Borrmann et al., 1996; Solomon et al., 1997). Contrary to the polar stratosphere where the persistence of PSC's is sufficient for complete heterogeneous processing of halogen containing reservoir molecules, the situation in the midlatitude upper troposphere is quite different. Natural or aviation-induced Cirrus clouds have a limited lifetime during which heterogeneous processing may occur. Borrmann et al. have assumed an average cloud lifetime of only 20 min which nevertheless led to a significant predicted impact on atmospheric chemistry. Therefore, the evaporative lifetime of Cirrus ice particles and the impact of atmospheric trace gas adsorbates such as HX on this lifetime are important parameters controlling the extent of heterogeneous processes.

For several years, a considerable number of studies on the kinetics of evaporation of H_2O on ice has been performed. Some of these studies have focused on the temperature dependence of the rates of evaporation and condensation of H_2O on pure ice using different techniques (Haynes et al., 1992; Brown et al., 1996; Chaix et al., 1998; Fraser et al., 2001). Others have mainly revealed the impact of trace gases of atmospheric importance on the evaporation rates, such as HNO_3 (Diehl et al., 1998; Warshawsky et al., 1999), HCl or

HBr (Hudson et al., 2001). The main result of these studies is the observation of the decrease of the rate of evaporation of H_2O (R_{ev}) on doped ice compared to R_{ev} on pure ice to variable extents. In this work both the kinetics of condensation (k_c) and evaporation (R_{ev}) have been measured under the same experimental conditions which has to our knowledge not been done before. The emphasis of the present work lies in the experimental separation of k_c and R_{ev} in order to obtain thermochemical closure with the H_2O vapor pressure over ice which imposes a powerful constraint on the separation of the rate of condensation and evaporation.

Several studies address the direct investigation of the condensed phase of H_2O in order to characterize the ice substrate using FTIR spectroscopy. Thus, the investigation of the IR absorption spectrum of pure ice has been undertaken (Schriver-Mazzuoli et al., 2000) in order to spectroscopically characterize the ice structure, as well as the impact of HNO_3, HCl and HBr deposition (Ritzhaupt et al., 1990; Delzeit et al., 1993; Koehler et al., 1993; Horn et al., 1997; Dominé et al., 2001; Zondlo et al., 2000; Hudson et al., 2001). This led to the discovery of different surface species owing either to the formation of stoichiometric hydrates or amorphous mixtures. Because most of the aforementioned experiments have been performed under UHV conditions, they have been limited to temperatures well below 220 K which is the characteristic temperature of the tropopause and is of interest here. Therefore, we have extended the temperature range to 240 K in the present work in order to address atmospheric conditions of the upper troposphere/lower stratosphere region.

2 Experimental apparatus

The present experiment is a stirred flow reactor equipped with triple diagnostics. It allows FTIR spectroscopic characterization of the ice substrate in transmission as well as observation of the changes of the condensed phase thickness based on HeNe interferometry at 632.8 nm. In addition, a residual gas mass spectrometer enables the monitoring of the partial pressures above the HX/Ice condensate. The experimental apparatus consists of a stainless steel cylindrical reactor of volume $V_r = 1750$ or 2450 cm^3, equipped with various inlets and electrical and optical feedthroughs including two $2''$ diameter NaCl windows to enable FTIR monitoring of the HX/Ice condensate. The reactor is pumped at the bottom by a turbomolecular-pump (VARIAN Turbo-300VHT, 250 l s^{-1} N_2) through a $6''$ diameter gate valve that is closed during experiment, thus isolating the upper (reactor) and lower chamber, the latter of which is monitored by a residual gas mass spectrometer (BALZERS Prisma QMS200). The liquid nitrogen cryostat, mounted on top of the reactor and externally heated using electrical cartridge heaters allows for accurate temperature control of the NaCl or Si optical window serving as the substrate for ice deposited from the vapor phase in the range $100 \leq T/K \leq 250$ (± 1 K). The ice temperature is periodically checked against the vapor pressure of H_2O over ice (Marti et al., 1993) using a type T thermocouple and a Baratron absolute pressure gauge (220-AHS). We would like to stress that in contrast to most other cryostats presently in use the Si window of 0.78 cm^2 cross section used as the substrate for the ice films is the only cold part of the chamber exposed to the gas phase (see Fig. 1). This has been checked in numerous experiments by correlating the loss of H_2O vapor by monitoring the pressure change in a Teflon (FEP)-coated calibrated volume used as a reservoir for the injection of H_2O molecules into the reactor with the number of molecules deposited on the Si window by monitoring the optical density in the IR spectral region and the integrated MS signal resulting from the evaporation of the ice film.

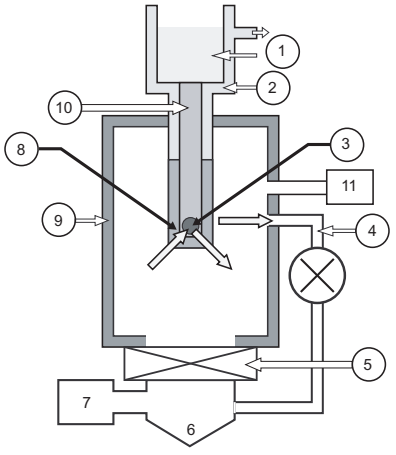

Fig. 1. Schematic drawing of the experiment:**1** Liquid nitrogen reservoir, **2** Evacuated Dewar vessel, **3** Silicon window of 0.78 cm^2 area used as a substrate for H_2O deposition, **4** Calibrated leak equipped with a valve allowing *static* (valve closed) and *stirred flow* (valve open) experiments, **5** 6"diameter gate valve, **6** Flange for Turbo Pump, **7** Quadrupole Mass spectrometer, **8** PTFE thermal insulation isolating the whole cryostat but the Silicon window which is the only low temperature part exposed to the gas phase, **9** Reactor chamber, **10** Solid copper finger with cartridge heaters for heating used to control the temperature of the Silicon Substrate, **11** Absolute pressure gauge (Baratron). Several type T thermocouples (not shown here) are located throughout the vacuum side of the cryostat in order to measure the temperature in different areas (Silicon window, PTFE Insulation, Reactor and Calibrated Leak walls,...). In addition, two $2''$ diameter NaCl windows allow the FTIR monitoring of the condensed phase, and two inlets allow the injection of H_2O as well as HX into the reactor. The hollow arrows describe the important kinetic processes taking place, such as adsorption, desorption and effusion of H_2O vapor.

Three types of measurements have been performed in the present experiment. The first is based on the use of a residual gas MS which is connected to the upper chamber both by a 6" diameter gate valve and a calibrated leak whose rate constant for effusion of H_2O and HCl at ambient temperature are $k_{esc}(H_2O) = 0.055$ s^{-1} and $k_{esc}(HCl) = 0.043$ s^{-1},

respectively. These values have been obtained from the evaluation of the exponential decrease of the pressure in the reactor measured using a 1 mbar full scale Baratron gauge (MKS Baratron pressure transducer Type 220AHS) when it is set from static to stirred flow condition by opening the calibrated leak valve. This leak allows the use of the reactor either under static conditions with the calibrated leak closed or as a stirred flow reactor with the leak valve open (see Fig. 1). It operates from the free molecular flow regime to the transition region up to a mbar or so of total pressure. In this latter configuration the range of water partial pressures (P_{H_2O}) in the upper chamber ranges from 10^{-4} to 1 mbar and is measured using the 1 mbar full scale Baratron gauge. For the remainder of this paper pressure units of Torr will be used throughout. The conversion of Torr to mbar may be performed using the relation 1 mbar = 0.75 Torr. The gas composition during an experiment is continuously monitored using the MS with the calibrated leak valve open.

The second diagnostic is based on a Fourier Transform Infrared Spectrometer (BIORAD FTS-575C) used in transmission across the Si window. It characterizes the composition changes of the condensed phase, which corresponds 1:1 to changes of the gas phase composition as the optical window is the coldest point of the whole reactor owing to extensive thermal insulation of the cryostat but the optical window. It was achieved using a tightly fitted PTFE sleeve whose temperature never got lower than approximately 260K for all experiments. Therefore, any change in the optical density of the deposited film due to evaporation or condensation in the static cryostat system is accompanied by a change in P_{H_2O} which can be monitored using either the partial pressure (MS) or the absolute pressure gauge. All the FTIR scans presented in this work have been recorded on a cryogenic mercury cadmium telluride detector using a resolution of 1 cm^{-1} and correspond to averaging of 4 consecutive scans.

The third diagnostic technique is based on He-Ne interferometry used to monitor changes of the thickness of the ice deposit with time. In such a configuration described elsewhere (Berland et al., 1994), the change of the thickness d_i is given by the relation

$$d_i = N_i \frac{\lambda}{2} \frac{1}{\sqrt{n_i^2 - \sin^2\theta}} \quad (1)$$

where d_i is the total change in thickness of the ice film, N_i the number of observed fringes, $\lambda = 632.8$nm the wavelength of the He-Ne laser, n_i the refractive index of vapor deposited ice set to n_i=1.3 and independent of T in the range 180–220 K (Berland et al., 1995), and $\theta = 12°$, the angle between the normal to the ice surface and the incident He-Ne beam. Using the appropriate parameters for the present cryostat one obtains $d_i = 246\times N_i$ nm which indicates a difference d_i in ice thickness of 246 nm between the homologous points of two adjacent interference fringes. This leads to the number of water molecules deposited on the substrate

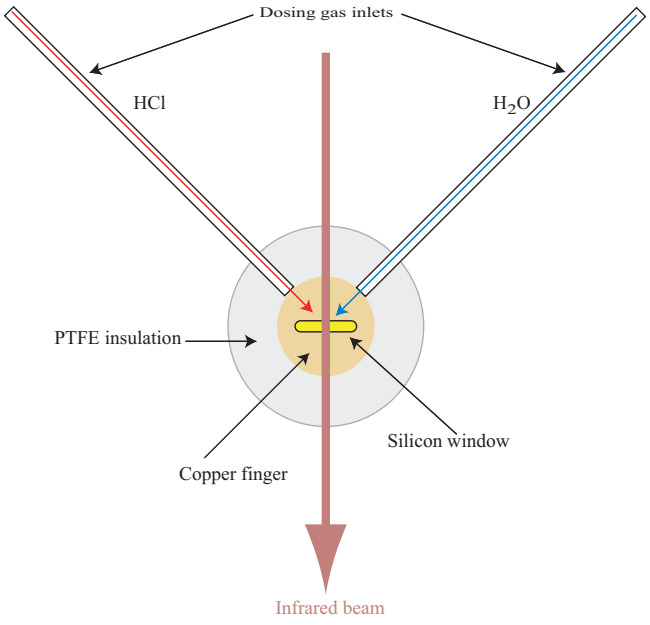

Fig. 2. Horizontal cut through dosing tubes and IR beam transmitted across the Si window. The PTFE-insulated copper finger of the cryostat is arranged perpendicularly to the reference plane.

of $N_{H_2O} = 6.2\times10^{17}\times N_i$ with the density of ice assumed to be constant and equal to 0.93 g cm^{-3} (Berland et al., 1995) in the range 180 to 220 K. The ice film is grown under static conditions by deposition from water vapor using bidistilled water at a typical rate of 10^{17} molecule s^{-1} by flowing H_2O vapor across a gas dosing tube directed towards the optical substrate. The mean ice thickness is approximately 1μm before HCl deposition starts.

Figure 2 presents a horizontal cut of the dosing arrangement whose plane contains the two dosing tubes as well as the IR beam transmitted across the Si window. The flat face of the Si window mounted at the lower end of the cryostat is perpendicular to the reference (paper) plane.

The measurement of the dose of HCl or HBr dispensed on the deposited ice film follows a two-pronged strategy which consists of (1) establishing the absolute flow rate of HX admitted into the cryostat chamber using MS signals under stirred flow conditions, and (2) integrating the amount of HCl lost by adsorption from the gas phase to the ice film, both by monitoring the gas phase using the residual gas MS as well as the condensed phase using FTIR transmission. Step (1) involves monitoring the MS signal at $m/e = 36$ for HCl and $m/e = 82$ for HBr, with the gate valve closed and the calibrated leak open thus enabling gas phase monitoring on-line under stirred flow condition. Previously, the MS signal intensities for HCl had been calibrated thus leading to a 1:1 relationship between the MS signals and the HCl concentration in the chamber. Using the known values of k_{esc} for HCl, the measurement of the partial pressure of the trace gas using the

Table 1. Data on experimental hardware configuration and results of calibrations. The sample surface area is A_s=0.78 cm^2

Experiment configuration	Reactor Temperature [K]	Reactor Volume [cm^3]	Collision frequency on ice [s^{-1}]		Rate of effusion for calibrated leak [s^{-1}]		Calculated escape orifice [mm^2]	HeNe angle [degree]	Thickness for one HeNe fringe [nm]	Thickness [nm] for FTIR OD=1.08	MS Calibration factor [molec s^{-1} A^{-1}]	
			H_2O	HCl	H_2O	HCl					H_2O	HCl
1	300	1750	6.52	4.62	0.2	0.13	2.4	12	246	1000	$5.80 \cdot 10^{24}$	$6.31 \cdot 10^{24}$
2	330	2450	4.89	3.46	0.055	0.043	0.8	12	246	1000	$5.70 \cdot 10^{23}$	$6.25 \cdot 10^{23}$

Baratron gauge in the cryostat chamber or the corresponding MS signal of HCl leads to the absolute flow rate in molec s^{-1} according to Eq. (2):

$$\text{FlowRate} = \frac{PV}{RT} k_{esc} = [HCl]\, V k_{esc} = C V k_{esc} P_{HCl} \quad (2)$$

where C is the conversion factor between partial pressure of HCl and HCl concentration in molec $Torr^{-1}$ cm^{-3} ($3.2 \cdot 10^{16}$ and $2.9 \cdot 10^{16}$ for configurations 1 and 2, respectively, displayed in Table 1), P_{HCl} the pressure of HCl in Torr, V the volume of the reactor and k_{esc} the rate of effusion of HCl through the calibrated leak in s^{-1} (see Table 1 for detailed information). The same technique has been used for all gases throughout this work. Moreover, the inlet made out of glass tubing and used for trace gas injection into the upper chamber is equipped with a micrometer dosing valve (Swagelok double pattern low-pressure metering valve with Vernier handle of type SS-SS2-D-TVVH) and is located between the calibrated volume used as a reservoir for HX and the inlet dosing tube, we have calibrated this valve by establishing the correspondence between the size of its aperture and the resulting MS signal, thus leading to an absolute calibration of the flow rate of HX molecules injected versus the aperture size of the micrometer dosing valve. Step (2) consists of integrating the absolute flow of HCl that was condensed onto the ice film in order to determine the HCl dose. As the window of the cryostat exposed to the gas is known to be the only part that is at low temperature during the experiment, the difference of the integrals of the MS signal of HX with the optical substrate at ambient temperature (no ice) and in the presence of an ice film, enables the evaluation of the absolute number of molecules deposited onto the ice.

In practice a dosing experiment takes place according to two different protocols depending on whether the temperature of the ice substrate is (a) T $\leq$ 190 K or (b) T $>$ 190 K. Under (a) the dosing experiment is performed under stirred flow conditions because the rate of H_2O evaporation is slow which limits its loss from the ice film during the experiment. At first the MS signal of HCl is recorded after turning on the HCl at constant flow rate for a given amount of time with the Si window at ambient temperature. Subsequently the same sequence is repeated with the Si window at low temperature. Figure 3 displays a typical experiment performed in order to obtain an absolute calibration of the HCl dose under these conditions. The dose corresponds to the hatched area pertaining to the difference of the integrals of the MS signals. When the dosing experiment is performed under high temperature conditions (b) the first step is identical and serves to establish the total number of HCl molecules dispensed with the Si window at ambient temperature. This experiment is now repeated with the Si window at T $>$ 190K and the gate valve closed, that is under static conditions, in order to prevent significant H_2O evaporation from the ice film at those higher temperatures. Although we are "blind" during the deposition of HCl onto the ice film owing to the static nature of the dosing the experiments discussed above reveal an exceedingly small HCl partial pressure in the chamber during the dosing so that we are confident about the HCl dosing even though we are unable to follow the HCl signal during the dosing. In practice more than 98% of the dispensed HCl molecules are adsorbed onto ice over the examined temperature range, a result that is also consistent with mass balance experiments discussed in more detail below.

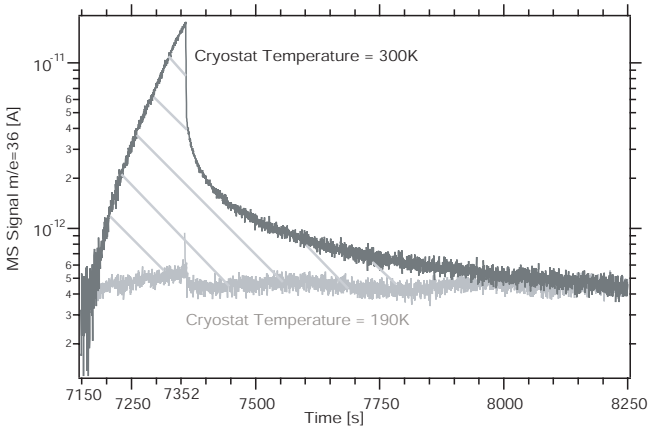

Fig. 3. Raw mass spectrometer signal for HCl at $m/e = 36$. The black and grey traces correspond to the reference signal with the cryostat at 300 K and 190 K in the presence of ice, respectively. At $t = 7150$ s, the HCl dosing valve is opened to the same extent in both cases, and is closed at $t = 7352$ s. In this example the total amount of HCl molecules disappearing from the gas phase is $(8 \pm 0.5) \cdot 10^{14}$ molecules and corresponds to the hatched area.

In support of the dosing procedure Table 2 displays the mass balance for six selected dosing experiments, namely

Table 2. HCl mass balance for 6 typical experiments

Experiment Number	Temperature (K)	HCl/Ice Structure	Number of HCl molecules deposited on ice (according to Fig. 3)	Number of HCl molecules desorbing from ice during evaporation of the ice film (based on MS changes)
1	180	HCl:6H_2O	8.7 10^{14}	8.4 10^{14}
2	180	Amorphous	2.1 10^{15}	2.0 10^{15}
3	180	Amorphous	4.3 10^{16}	3.6 10^{16}
4	190	HCl:6H_2O	1.1 10^{15}	1.1 10^{15}
5	190	HCl:6H_2O	1.0 10^{15}	9.8 10^{14}
6	190	Amorphous	2.0 10^{15}	1.7 10^{15}

that between HCl dispensed to the ice substrate (column 4 of Table 2) and the HCl recovered after complete H_2O and HCl evaporation (column 5 of Table 2) once the sample support has reached ambient temperature. The excellent mass balance validates the chosen dosing procedure, in particular it refutes the possibility that the chamber walls act as a significant reservoir for HCl.

The smallest measurable MS signal level at $m/e = 36$ within an acceptable S/N ratio of our apparatus is on the order of 3×10^{-13}A with a rise time of nearly 10 s. This leads to an estimate of $2 \cdot 10^{12}$ molecules corresponding to $3 \cdot 10^{-3}$ of a formal monolayer using a calibration factor for the MS signal of 6.25×10^{23} molec $s^{-1}A^{-1}$ for the smallest measurable amount of HCl deposited on the optical substrate. The lowest achievable deposition rate was $2 \cdot 10^{11}$ molec s^{-1} and the lowest detectable partial pressure of HCl monitored by residual gas MS was of the order of $6 \cdot 10^{-8}$ Torr. We have estimated that owing to the very small gas phase density of HCl in the presence of an ice film of typically $8 \cdot 10^{-8}$ Torr the adsorption of gas phase HCl would take a time exceeding the typical duration of the present experiments. We have therefore ignored the deposition rate of HCl onto the ice sample under HCl background conditions afforded by the maximum pumping speed of the vacuum chamber.

An alternate method of dosing of HX onto the ice has been performed by the deposition of the trace gas under static conditions by backfilling the reactor volume with a measured amount of trace gas in addition to the method presented above which is the directed deposition of pure HCl onto ice across dosing tubes. No significant differences in the kinetic results have been observed when comparing the backfilling with the directed deposition technique. For HBr the present experimental setup does not allow quantitative dosing experiments because the PTFE insulation apparently irreversibly adsorbs small quantities of HBr. However, the used deposition settings for HBr were identical to the ones used for HCl allowing the estimation of upper limits for the concentration of HBr.

3 Results

Both the rate of evaporation R_{ev} in molec s^{-1} cm^{-3} and the uptake coefficient γ of H_2O vapor uptake on ice have been measured between 200 and 240 K for pure ice and in the presence of known amounts of HCl or upper limited amounts of HBr according to the net reaction:

$$H_2O(g) \underset{R_{ev}}{\overset{k_{\mathrm{cond}}}{\rightleftharpoons}} H_2O(\text{bulk ice}) \tag{3}$$

with γ=k_{cond}/ω, where k_{cond} is the condensation rate coefficient in s^{-1} and ω is the collision frequency of H_2O with the ice film in s^{-1} (see Table 1). Both the rate of evaporation R_{ev} and the rate of condensation R_{cond}= k_{cond} [H_2O] are expressed in units of molec s^{-1} cm^{-3} and address the gain and loss, respectively, of H_2O vapor with respect to the gas phase. Both processes may also be expressed in terms of fluxes of gas phase molecules to and from the substrate surface. The rate R_{ev} and flux J_{ev} of evaporation are connected through the relationship J_{ev}=R_{ev}/(A_s/ V), where (A_s/V) is the surface-to-volume ratio of the used experimental arrangement (see Table 1). Both rates and fluxes express the same physicochemical process, the rate being normalized for unit cm^3, the flux for unit cm^2 of substrate surface.

The separation of the rate of evaporation and condensation was enabled by using a method which consisted of the consecutive use of the reactor in the static and the stirred flow mode. By measuring P_{eq}, the equilibrium H_2O vapor pressure in the reactor (upper chamber) under static condition, and P_{ss}, its corresponding steady state partial pressure under stirred flow condition, R_{ev} and k_{cond} were calculated using the following equations:

$$P_{eq} = \frac{R_{ev}}{k_{\mathrm{cond}}} \times RT \qquad P_{ss} = \frac{P_{eq}}{\frac{k_{esc}}{k_{\mathrm{cond}}} + 1} \tag{4}$$

In all experiments presented in this work ice was always deposited at 190 K at a rate of 10^{17} molec s^{-1} and heated to the desired temperature after deposition. Both P_{eq} and P_{ss} have been corrected for the fact that the colliding gas, namely water vapor, was at ambient or slightly higher temperature

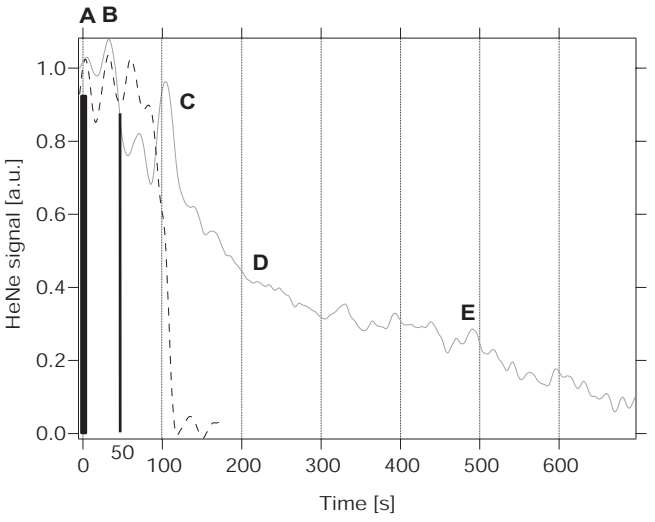

Fig. 4. Interferometric signal of evaporating: **(a)** pure ice (black dashed), **(b)** HCl-doped ice film of 10^{15} deposited HCl at 190K (gray). At $t = 0$, the static system is set to stirred flow condition by opening the leak valve (first black vertical line). The second vertical line corresponds to the first noticeable difference between interferograms.

as it is controlled by the temperature of the chamber walls whereas the target consisting of the ice film deposited on the optical support was at low temperature. Under those conditions both the pressures, P_{eq} and P_{ss}, as well as [H_2O] are related to the measured values by both the temperature of the cold target and the chamber walls at ambient temperature. The correction procedure valid for the molecular flow regime is explained in more detail in Annex A.

The protocol for the deposition of ice leading to samples of typically 1μm thickness was kept the same throughout the present study. The deposition temperature of 190 K was deliberately chosen so as to lead to the formation of thermodynamically stable polycrystalline ice of hexagonal I_h crystal structure thus minimizing the occurrence of mixtures with cubic and amorphous phases that are metastable at 190 K. A mixture of ice phases may lead to a H-bonding environment that is different compared to the thermodynamically stable pure ice phase I_h crystal structure as has been shown by Schaff and Roberts (1996) using FTIR reflection-absorption spectroscopy. In addition, we may exclude the presence of a significant degree of porosity in the present ice films as shown by Keyser et al. (1992). We have therefore chosen an ice deposition protocol that should always lead to a homogeneous film of thermodynamically stable I_h crystal structure irrespective of the temperature of the film used for further investigations.

A known quantity (dose) of HX was subsequently deposited on the pure ice film, and both the equilibrium vapor pressure P_{eq} of H_2O as well as its steady state value P_{ss} were measured using the absolute pressure gauge or the MS signal for P_{ss}. This allowed the determination of R_{ev} and γ of H_2O in the presence of HX in comparison with pure ice. The number of HCl molecules adsorbed on the ice was in the range $10^{13} - 10^{15}$ molecules corresponding approximately to 0.01 to 1 formal monolayer with an upper limit of the HCl deposition rate of 10^{14} molec s^{-1}. For HBr the number of molecules adsorbed and the deposition rate are similar to HCl as only limiting values can be given (see above). During the measurement of P_{ss} of H_2O no HX desorption has been observed while H_2O was evaporating from the ice, and a change in $m/e = 36$ and 82 for HCl and HBr, respectively, was only observable during the evaporation of the last few tens of nm film thickness as observed by simultaneous monitoring of the change in thickness of the ice deposit and the gas phase composition using HeNe interferometry and MS, respectively. One must keep in mind that steady state conditions for H_2O, P_{ss}, in the case of doped ice were attained once a significant fraction of the ice sample evaporated in contrast to pure ice where steady state conditions are attained instantaneously. The remaining thickness corresponded to the last few hundred nanometers of ice between points **C** and **D** of the HeNe interferogram displayed in Fig. 4 corresponding to 25–50% of the thickness of the original ice film. Thus the mean HCl mole fraction in the remaining ice film was in the range $3.2 \cdot 10^{-5}$ to $6.4 \cdot 10^{-5}$ for a dose of 10^{13} adsorbed HCl molecules, and between $3.2 \cdot 10^{-3}$ and $6.4 \cdot 10^{-3}$ for a dose of 10^{15} adsorbed HCl. The latter case corresponds to the situation between points **C** and **D** of the displayed HeNe interferogram in Fig. 4 and suggests that one adsorbed HCl molecule may exert a significant kinetic effect on roughly 500 H_2O molecules.

The kinetic results are shown in Figs. 5 and 6 which display J_{ev}, the evaporative flux and γ, the uptake coefficient. It is important to point out that in the presence of a dose of adsorbed HX in the range given above, the measured equilibrium vapor pressure P_{eq} of H_2O(g) is that over pure ice and therefore independent of the doses of HX over the range explored. Figure 5 shows the decrease of J_{ev} in the presence of HCl relative to that of pure ice by a factor of 3 to 6 at doses smaller than 10^{15} molec cm^{-2} corresponding to one formal monolayer or less of HCl. The uptake coefficient γ displayed in Fig. 6 undergoes the same change as J_{ev} owing to the constraint that the measured P_{H_2O} is that of pure ice. This decrease in J_{ev} and γ depends upon the number of HCl molecules deposited on the surface of the ice, but stays constant for amounts larger than 10^{14} molecules of HCl adsorbed on ice as displayed in Fig. 7. It shows the HCl dose dependence of J_{ev} together with a discontinuity around $6{\cdot}10^{13}$ of deposited HCl molecules which corresponds to a mole fraction for HCl in ice between $1.9 \cdot 10^{-4}$ and $3.8 \cdot 10^{-4}$. It seems that for doses of deposited HCl up to $1{\cdot}10^{14}$, J_{ev} stabilizes around $5{\cdot}10^{16}$ molec cm^{-2} s^{-1} which is the value displayed in Fig. 5 at 210 K. However for larger doses of HCl both J_{ev} and γ continue to decrease. Figures 5 and 6 display all values obtained in this work including the ones at very large HCl doses (inverted triangles in Figs. 5 and 6).

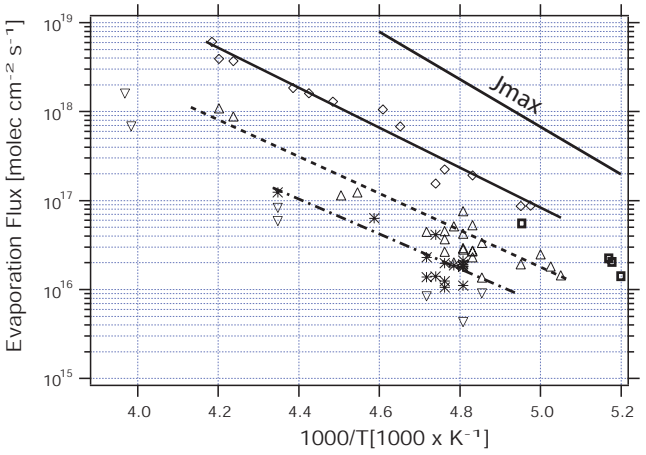

Fig. 5. Arrhenius plot of the evaporative flux of H_2O (J_{ev}) from pure and HX doped ice films (□: condensed ice, Chaix et al., 1998; ◇: condensed ice, this work; △: HCl-doped ice, this work; ✳: HBr-doped ice, this work). The typical uncertainty of individual points are within the size of the symbols. ∇: value observed for a very large dose of HCl leading to the formation of a liquid HCl/H_2O mixture on the ice surface. J_{max} corresponds to the theoretical maximum value for the evaporative flux of a pure ice film ($\gamma = 1$).

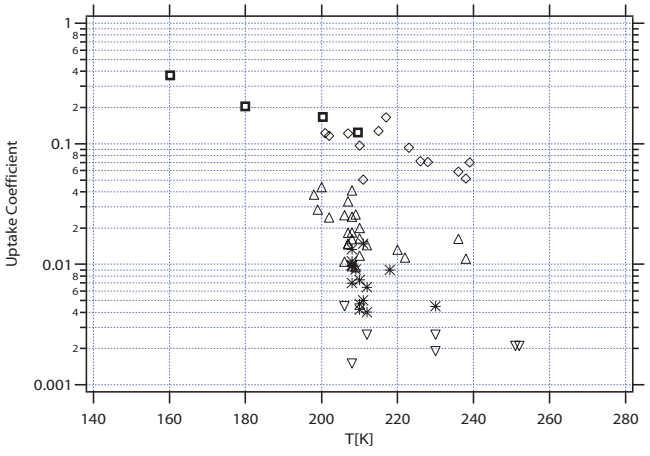

Fig. 6. Temperature dependence of the uptake coefficient γ of H_2O from pure and HX-doped ice films (□: condensed ice, Chaix et al., 1998; ◇: condensed ice, this work; △: HCl-doped ice, this work; ✳: HBr-doped ice, this work. ∇: value observed for a very large dose of HCl leading to the formation of a liquid HCl/H_2O mixture on the ice surface.)

The energy of activation for the flux of evaporation, J_{ev}, and the rate constant for condensation, k_{cond} of H_2O from pure ice is calculated to be $E_{ev} = 10.3 \pm 1.2$ kcal mol^{-1} and $E_{cond} = -1.6 \pm 1.5$ kcal mol^{-1}, respectively, leading to the Arrhenius expression $J_{ev} = 1.6 \cdot 10^{28\pm1} \cdot \exp\left(\frac{-10.3\pm1.2}{RT}\right)$ [molec cm^{-2} s^{-1}] and $k_{cond} = \left(1.7 \cdot 10^{-2\pm1}\right) \cdot \exp\left(\frac{+1.6\pm1.5}{RT}\right)$ [s^{-1}] for the range 200 to 240 K.

For HCl doped-ice the values are $E_{ev} = 9.7 \pm 1.2$ kcal mol^{-1} and $E_{cond} = -1.5 \pm 1.6$ kcal mol^{-1} leading to $J_{ev} = 6.4 \cdot 10^{26\pm1} \cdot \exp\left(\frac{-9.7\pm1.2}{RT}\right)$ [molec cm^{-2} s^{-1}] and $k_{cond} = \left(2.8 \cdot 10^{-3\pm1}\right) \cdot \exp\left(\frac{+1.5\pm1.6}{RT}\right)$ [s^{-1}] for the range 200 to 240 K.

In the presence of HBr, the decrease of J_{ev} is more important than for HCl and J_{ev} is almost 20 times smaller than on pure ice for similar estimated doses of HBr. This led to an activation energy of H_2O evaporation and condensation from HBr-doped ice of $E_{ev} = 9.1 \pm 1.2$ kcal mol^{-1} and $E_{cond} = -2.6 \pm 1.6$ kcal mol^{-1}, respectively, leading to $J_{ev} = 7.4 \cdot 10^{25\pm1} \cdot \exp\left(\frac{-9.1\pm1.2}{RT}\right)$ [molec cm^{-2} s^{-1}] and $k_{cond} = \left(7.1 \cdot 10^{-5\pm1}\right) \cdot \exp\left(\frac{+2.6\pm1.5}{RT}\right)$ [s^{-1}] in the range 200 to 240 K. Following these results, the decrease of the pre-exponential factor in J_{ev} is responsible for the most part for the change of the rate of evaporation of H_2O thus leaving the exponential factor unchanged within experimental uncertainty.

Observations of the condensed phase in the absence and the presence of HCl have also been performed using HeNe interferometry simultaneously with MS and FTIR measurements. Figure 4 shows the decrease of the thickness of a 1 μm thick slab of pure and HCl-doped ice at 190 K with time. First, the ice film is grown under static conditions, and is subsequently doped with 10^{15} molecules of HCl or HBr. The decrease in the net rate of H_2O evaporation of the 1 μm thick ice film in the presence of 10^{15} deposited HCl molecules corresponding to less than 2 monolayers amounts to a factor of 5 to 6 compared to pure ice once steady state is achieved between points **C** and **D** and maintained to point **E**. This is also the time period during which P_{ss} (Eq. 4) has been measured. The portion of the interferogram between $t = 100$ and 300 s in Fig. 4 containing points **C** and **D** describes a sinusoidal change of the photodiode signal which in turn corresponds to a linear change of thickness with time according to Eq. (1). This result is in good agreement with the decrease of R_{ev} observed in the presence of HCl discussed above, albeit not directly comparable. The observation of the condensed phase implies a **net** change, that is the difference between evaporation and condensation rate whereas the gas phase measurement results in separate kinetic rates R_{ev} and $k_{cond}[H_2O]_{SS}$. The net change observed interferometrically is somewhat less than the change based on R_{ev} alone within a factor of two as condensation of H_2O onto the remaining ice film counteracts the decrease of the thickness owing to R_{ev}.

One may note that the spacing between the interferometric fringes is gradually becoming larger which corresponds to a decrease of the net rate of evaporation starting around $t = 50$ s as shown in Fig. 4, point **B**, where $1.5 \cdot 10^{18}$ molecules of H_2O still remain in the ice film compared to

Table 3. Experimental observations of the HeNe interferogram during the evaporation of a 1μm thick pure ice film, as well as doped with HCl, under stirred flow conditions and for different doping conditions. Cases (a), (b), (c) correspond to experimental configuration 1 (Table 1), cases (a') and (b') to configuration 2 (Table 1)

Ice Substrate Temperature [K]	Ice Thickness at deposition time [nm]	Dose of HCl molecules	Rate of deposition [molec s^{-1}]	Time for complete film evaporation [s]	Last 4 periods between fringes [s] 1	2	3	4	Trapped H_2O molecules	FTIR Spectral characterization at fringe 4
(a) 180	1000	Pure Ice	Null	217	67	60	50	40	Null	Pure Ice
(b) 180	1000	$1 \cdot 10^{15}$	$1 \cdot 10^{13}$	320	74	69	58	**116**	$1.5 \cdot 10^{18}$	HCl:6H_2O
(c) 190	1000	$1 \cdot 10^{15}$	$6 \cdot 10^{12}$	450	73	75	**120**	**160**	$2.5 \cdot 10^{18}$	Amorphous HCl:H_2O
(a') 190	1000	Pure Ice	Null	125	30	30	30	35	Null	Pure Ice
(b') 190	1000	$1 \cdot 10^{15}$	$1 \cdot 10^{13}$	708	35	35	38	**600**	$1.5 \cdot 10^{18}$	HCl:6H_2O

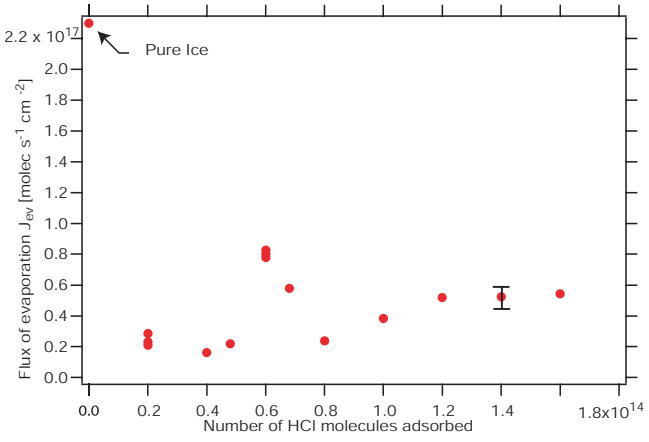

Fig. 7. Dependence of J_{ev} on the number of HCl molecules adsorbed on 0.78 cm^2 of ice substrate at 210 K. The stable level appearing for a dose higher than $1 \cdot 10^{14}$ molecules was chosen for the data displayed in Fig. 5.

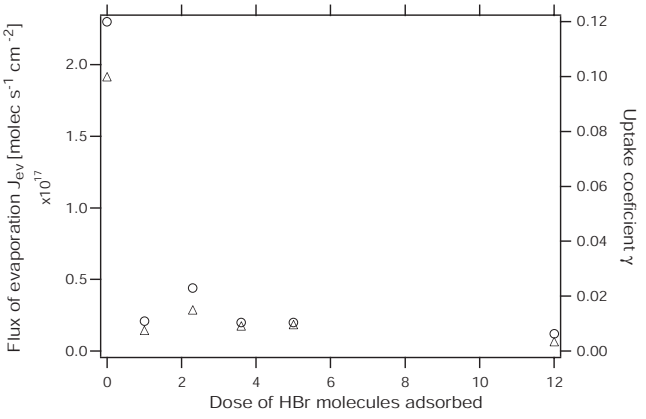

Fig. 8. Dependence of J_{ev} (○) and γ (△) on the number of HBr molecules adsorbed on the ice surface at 210 K. The stable level for a dose higher than 3.6 was used in Fig. 5. A dose of 1 corresponds to a maximum of $5 \cdot 10^{16}$ molecules adsorbed.

$2.5 \cdot 10^{18}$ at the beginning of the evaporation corresponding to roughly 50% of the original ice film thickness. As no desorption of HX from the film was observed using MS, we therefore claim that the amount of HX adsorbed on the ice film is responsible for this change of J_{ev} as discussed above. At first only the H_2O molecules that are not influenced by the presence of HX are evaporating at the characteristic rate of pure ice which corresponds to the portion of the interferogram of Fig. 4 between points **A** and **B**. The presence of adsorbed HCl molecules therefore does not hinder H_2O molecules from the deeper hence pure portion of the ice film to evaporate as if it were a pure ice sample. Between points **B** and **E** of the interferogram the decrease of the rate of evaporation of H_2O is due to the effect of HX on the water molecules making up the remainder of the ice substrate. The presence of HX is being felt more strongly with time by the remaining H_2O molecules as the mole fraction of HX in ice becomes more important owing to the fact that only H_2O but no HCl is desorbing. This results in an upper limit value of $\chi_{HCl} = 1.2 \cdot 10^{-2}$ at point **E** in Fig. 4. This means that one molecule of HCl exerts a significant kinetic influence on roughly 100 H_2O molecules. From point **E** of the interferogram to the end of the evaporation of the film we have observed HCl in the gas phase using MS detection.

Table 3 displays some typical observations of the temporal evolution of the HeNe interferogram for different doping conditions of the ice film under stirred flow conditions. Case (a), (b) and (c) refer to one experimental configuration, whereas cases (a') and (b') differ from the former by a change of the calibrated leak. The comparison between (a) and (b), on the one hand, and (a') and (b') on the other hand illustrates the conclusions cited above concerning the change in the net rate of H_2O evaporation from ice in the presence of HCl. In the cases (b), (c) and (b') corresponding to HCl doping the evaporation rate for 50 to 75% of the film thickness is that of pure ice and therefore not affected by the presence of $1 \cdot 10^{15}$ HCl molecules. Cases (c) and (b') make for an interesting comparison. The stable hydrate

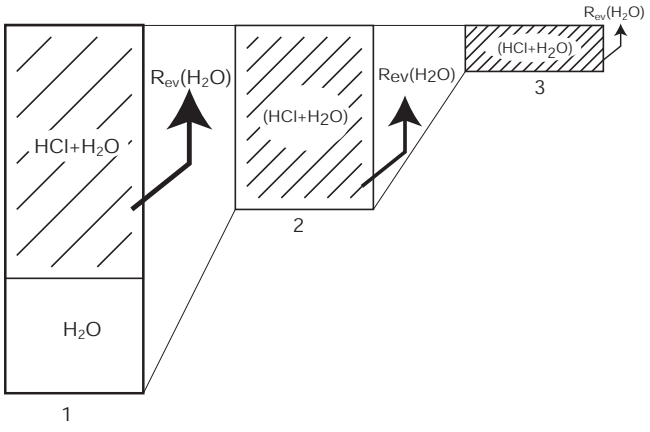

Fig. 9. Cartoon of the fate of a HCl-doped ice film upon evaporation of H_2O (see text for explanation). Hatched areas represent the mixture of HCl/H_2O

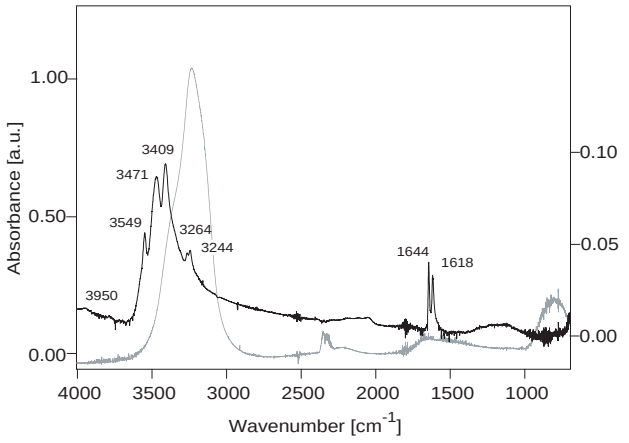

Fig. 10. FTIR absorption spectrum of pure (grey, left scale) and HCl-doped ice (black, right scale). Both traces are rescaled for legibility. The ice film is doped with 10^{15} molecules of HCl at a flow rate of 10^{13}molec s^{-1}.

$HCl{:}6H_2O$ (case (b')), whose formation will be discussed below, significantly slows down the net rate of evaporation, say by a factor of less than 20 corresponding to 600 vs. 35 s per fringe which is the time needed to evaporate an ice film thickness of 246 nm corresponding to one interference fringe of the HeNe interferogram. However, the crystalline hydrate (case (b')) extends just over one fringe at the used HCl dose whereas the presence of the amorphous hydrate (case (c)) affects 50% of the sample thickness as it is apparently distributed in a more diffuse manner across the ice sample. In contrast its presence affects the H_2O evaporation rate to a lesser extent corresponding to a decrease of a factor between 2 and 3. We would like to stress, however, that the resolution of the HeNe interferogram is too crude in order to draw quantitative conclusions in the present case. We just underline the qualitatively similar conclusions between the interferometric and the quantitative kinetic results obtained from gas phase observations and discussed above. For HBr doping, the decrease in the net rate of evaporation as observed from the corresponding interferogram is on the order of 30 to 40 for HBr levels similar to HCl which is within a factor of two of the results on R_{ev} discussed above (Fig. 5). One needs to be reminded, however, that in contrast to the measurement of R_{ev} presented above the observation of the change in ice film thickness addresses the net rate of evaporation and is therefore smaller than R_{ev} at a given partial pressure of H_2O.

The FTIR absorption spectroscopic study has led to four sets of results that have been obtained at 190 K on a 1μm thick ice film and which are summarized in Table 4.

Figure 9 presents a cartoon describing these processes where **1** corresponds to the composition of the substrate within the time period between **A** and **B** of the interferogram, **2** to the period between **B** and **C** and **3** to the period between **C** and **E**. However, it does not differentiate between cases (c) and (b), (b)' displayed in Table 3, namely between the amorphous HCl/H_2O mixture and the crystalline hexahydrate, respectively. The spatial extent of the phase containing HCl is summarily earmarked by bold numbers in Table 3. Interestingly, the spatial extent of the amorphous phase is larger by roughly a factor of two compared to the crystalline HCl hexahydrate, the latter of which seems to be a more compact layer compared to the former. Nevertheless, the evaporation of pure underlying H_2O seems to go on unabatedly at the evaporation rate characteristic of pure ice regardless of the nature of the "capping" phases. This result is in stark contrast to the conclusions presented by Biermann et al. (1998) and highlights the effect that small doses of HCl in the range of one to two formal monolayers may have on the kinetics of condensation and evaporation of H_2O. However, this contaminated layer of ice does not seem to constitute a barrier for the evaporation of the underlying pure ice.

First, the spectrum of pure ice in Fig. 10 reveals the presence of polycrystalline I_h ice in the OH-stretch region as discussed previously. The spectrum shows an absorption peak at 3230 cm^{-1} with shoulders at 3150 and 3350 cm^{-1} (Bergren et al., 1978) which is expected from previous work on films deposited at temperatures higher than 180 K (Kumai, 1968). For a dose of less than 10^{13} molecules of HCl deposited at a rate of less than 10^{13} molec s^{-1} (Table 4, case a), no change in optical density was observed across the entire IR absorption spectrum from 700 to 4000 cm^{-1} which remained that of pure ice. However, the presence of HCl on ice was ascertained by the decrease of J_{ev} of H_2O as described above. For a dose of HCl of more than 10^{14} molecules that is evaluated from the integral under the measured MS signal of HCl as displayed in Fig. 3 and a deposition rate of more than 10^{14} molec s^{-1} (Table 4, case d) the formation of an amorphous $HCl{:}H_2O$ mixture was observed whose absorption spectrum

Table 4. FTIR spectral observations of a 1μm thick ice film doped with HCl using different dosing protocols at 190 K

	a)	*b*)	*c*)	*d*)
Dose (molecule)	Low $< 10^{13}$	5.10^{13} to 10^{15}	5.10^{13} to 10^{15}	$> 10^{14}$
Flow rate (molec s^{-1})	Low $< 10^{13}$	10^{13} to 5.10^{13}	Low $< 10^{13}$	Large $> 10^{14}$
Spectral observation	No absorption attributable to HCl	3230 cm^{-1} Split+ shift Sharp 1644 and 1618 cm^{-1}	3250 cm^{-1} broadening 1100 and 1700 cm^{-1} absorption	3250 cm^{-1} broadening 1100 and 1700 cm^{-1} absorption
Identification	FTIR absorption spectrum is that of pure ice	Crystalline HCl hexahydrate (Fig. 10)	Amorphous $HCl:H_2O$ mixture (Fig. 11)	Amorphous $HCl:H_2O$ mixture (Fig. 11)

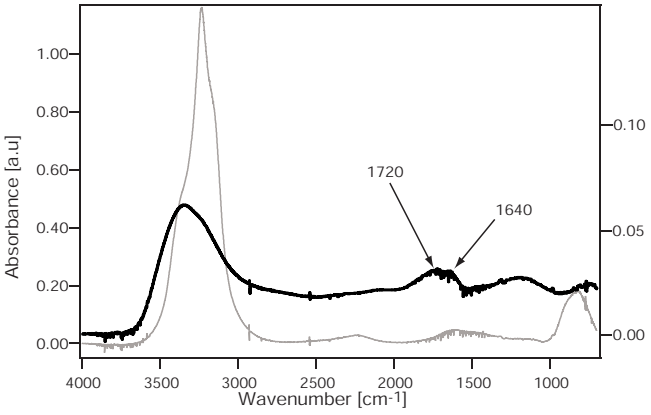

Fig. 11. FTIR absorption spectrum of pure (grey, left scale) and HCl-doped ice (black, right scale). Both traces are rescaled for legibility. The ice film is doped with 10^{15} molecules of HCl at a flow rate higher than 10^{14}molec s^{-1}.

is in agreement with results found in the literature (Dominé et al., 2001).

The obtained spectra for amorphous $HCl:H_2O$ mixtures are displayed in Fig. 11 and are in good agreement with the literature (Ritzhaupt et al., 1990). They are characterized by the appearance of new peaks between 1100 and 1200 as well as at 1700 cm^{-1} and by the broadening of the sharp OH-stretch band leading to a broad absorption around 3250 cm^{-1}. Ritzhaupt et al. (1990) have identified a stretching vibration of H_3O^+ at 1079 cm^{-1} whereas H_2O bending and H_3O^+ bond deformation modes contribute to the absorption at 1696 cm^{-1} in their FTIR absorption spectra. Koch et al. (1997) attribute a 1250 cm^{-1} band to the H_3O^+ stretching mode and a 1780 cm^{-1} vibration to the H_2O and H_3O^+ deformation mode. We therefore follow these assignments in this work and identify the broad absorption band centered at approximately 1100 cm^{-1} in Figs. 10 and 11 with the presence of H_3O^+. The sharp absorptions at 1618 and 1644 cm^{-1} in the case of the HCl hexahydrate (Fig. 10) as well as the broader peaks centered at 1640 and 1720 cm^{-1} in the case of the amorphous $HCl:H_2O$ mixture (Fig. 11), whose IR bands are broadened throughout the IR absorption spectrum in line with the amorphous nature of the absorber, point to the activity of the bending and deformation modes in H_2O and H_3O^+, respectively. Although no proof in itself, we claim that the significant intensity of these absorptions points towards the existence of ionic HCl hydrates of the form $H_3O^+Cl^-$ being present on ice in the temperature range investigated as no hint of molecularly adsorbed HCl could be found in the region of the H-Cl stretching vibration in the covered temperature range.

The most interesting result of these deposition experiments is the ability to control the growth of the crystalline HCl hexahydrate $HCl{\cdot}6H_2O$ at 190 K presented as case (b) displayed in Table 4. Figure 10 presents a FTIR absorption spectrum corresponding to case (b), where the ice film was doped with 10^{15} HCl molecules at a flow rate of 10^{13} molec s^{-1}. The presence of crystalline $HCl{\cdot}6H_2O$ is characterized by the shift and split of the 3230 cm^{-1} peak representative of the pure ice OH-stretch, and by the appearance of sharp peaks at 1644 cm^{-1} and 1618 cm^{-1} discussed above (Ritzhaupt et al., 1990). The spectrum of Fig. 10 corresponds to the deposition conditions of case (b) displayed in Table 4 and reveals the formation of a crystalline ionic hydrate of HCl with ice in agreement with the literature (Koch et al., 1997; Uras-Aytemiz et al., 2001) and with theoretical studies (Kroes et al., 1992; Gertner et al., 1996; Svanberg et al., 2000). We point out that this spectrum has been measured at a time in the film evaporation history that corresponds to the time interval given by points **B** and **D** of the interferogram displayed in Fig. 4 where all of the free water molecules constituting the underlying pure ice film have evaporated. This explains the importance of the FTIR absorptions attributed to the presence of the hydrates compared to the pure ice OH-stretch around 3230 cm^{-1} as all other H_2O molecules not involved in crystalline hydrate formation have evaporated leaving behind the "bare essentials" of the stable crystalline hydrate. The fact that the (almost) unperturbed ice OH-stretch at 3244 and 3264 cm^{-1} (compared to 3230 cm^{-1} in pure ice) is still observable at this stage of the evaporation attests to the presence of weakly-bound water molecules not involved in the formation of the hydrates although both their rate of

evaporation and condensation are influenced by the presence of HCl as indicated by their slight shift in the IR absorption spectrum.

The results are consistent with the fact that HCl hydrates have a H_2O vapor pressure that is lower than that of pure ice although it has not been measured in this work. It is also important to notice that the IR absorption peaks corresponding to the presence of HCl hydrates were also observable down to a dose of $5 \cdot 10^{13}$ molecules of HCl towards the end of an evaporation experiment. This HCl dose corresponds to approximately 10% of a formal monolayer of HCl on ice. At the beginning of the evaporation experiment the crystalline hydrate structure was not apparent perhaps because of the abundance of "pure" ice whose absorption spectrum is centered at 3230 cm^{-1} (Fig. 10). After most of the ice film evaporated at the rate characteristic of pure ice the remaining sample was monitored using the disappearance of the spectral fingerprints of the hydrates as given in Fig. 10. At this time the average mole fraction of HCl in ice was between $1.6 \cdot 10^{-4}$ and $3.2 \cdot 10^{-4}$ as indicated by the volume of remaining ice monitored by the interferogram for the time period between **C** and **D** of Fig. 4. We are unable at this point to determine the defining moments of the crystallization of the HCl hexahydrate. If it crystallized already at the end of the doping process the sensitivity of the FTIR absorption spectrometer in transmission may not have been sufficient to monitor the characteristic features of the crystalline HCl hexahydrate at 3549, 3471 and 3409 cm^{-1}. On the other hand, crystallization as probed by the appearance of the sharp hydrate structure in the OH-stretching region may have occurred when most of the pure ice had evaporated and the HCl concurrently concentrated at the interface thus enabling crystallization. This process would closely resemble the crystallization of nitric acid hydrates (NAT = $3H_2O{\cdot}HNO_3$, NAD = $2H_2O{\cdot}HNO_3$) under laboratory conditions as observed by Tolbert and coworkers (Zondlo et al., 2000).

A surprising case is (c) in Table 4 which indicates the absence of crystalline $HCl{\cdot}6H_2O$ and reveals that the formation of the crystalline hexahydrate depends on the rate of HCl deposition rather than on the HCl dose. For very low deposition rates of less than 10^{13} molec s^{-1} one concludes that the diffusion of HCl in ice is presumably faster than crystallization preventing the formation of the HCl hexahydrate. At the other extreme of a large deposition rate (case (d) in Table 4) formation of an amorphous HCl/H_2O mixture is preferred over formation of crystalline hexahydrate. Whatever the reason, it seems that at 190 K both the crystalline and amorphous HCl hydrates may be observed depending on the rate of deposition of HCl on ice. This case is of importance because the change in the net rate of evaporation seems to depend on the presence or absence of crystalline hydrates as displayed in Table 3, cases (c) and (b'). More importantly, the formation of these crystalline hydrates observed by FTIR absorption spectroscopy has a large impact on the rate of H_2O evaporation for a sample comprising the last 100 to 200 nanometers of ice whereas in the case of the formation of an amorphous $HCl:H_2O$ this impact is less which may be an indication of the importance of diffusion of HCl in the formation of the crystalline hydrates. Table 3 qualitatively shows the difference of the impact of the presence of $HCl{\cdot}6H_2O$ (case (b')) vs. amorphous $HCl:H_2O$ mixture (case (c)) as far as the temporal spacing between the interference fringes that are related to the net evaporation rate of H_2O are concerned. It also shows the difference in spatial extent (volume) of the HCl/H_2O layer discussed above.

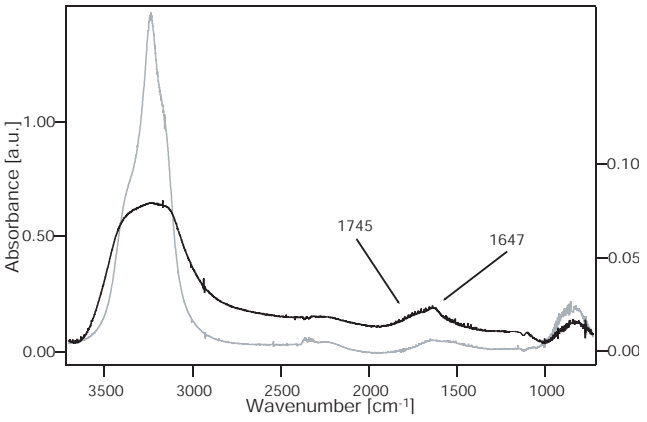

Fig. 12. FTIR absorption spectrum of pure (grey, left scale) and HBr-doped ice (black, right scale). Both traces are rescaled for legibility. The ice film is doped with an unknown amount of HBr.

For ice films doped with HBr, we have not been able to observe any spectral changes in the pure ice spectrum except for a broadening of the absorption due to the OH-stretch region and a shift of the 1641 cm^{-1} peak as displayed in Fig. 12 (Koehler et al., 1993). This is assigned to the bending mode of H_2O which is shifted to 1745 cm^{-1} upon HBr adsorption and is attributed to the H_3O^+ bending mode. This observation suggests complete ionization of HBr and is in agreement with the literature (Barone et al.,1999; Hudson et al., 2001). However, similar to the case of HCl, where no spectral change was observed (case a, Table 4) the presence of HBr was ascertained by the measurement of the decrease of J_{ev} of H_2O, as presented in Fig. 5.

4 Discussion and atmospheric implications

This experiment has enabled the separation of the rate or flux of evaporation R_{ev} or J_{ev} and the rate constant for condensation k_{cond} of H_2O from pure and doped water ice under the same experimental conditions. The separate rates and especially their temperature dependence have shed light on a complex adsorption/desorption mechanism as evidenced by the negative temperature dependence of k_{cond} as has been pointed out by Flückiger et al. (2003). The resulting value for the enthalpy of sublimation of H_2O from pure wa-

ter ice deduced from Arrhenius expressions given above is $\Delta H_{subl} = E_{ev} - E_{cond} = 11.9 \pm 2.7$ kcal mol^{-1} which is in good agreement with values found in the literature (Haynes et al, 1992; Fraser et al, 2001, Koehler, 2001). In contrast to most other results found in the literature, we assert that H_2O condensation on ice has a small negative activation energy in the range studied (190–240 K). The study of R_{ev} alone is therefore a necessary, but not sufficient condition to assess ΔH_{subl} or the binding energy of H_2O on ice at temperatures in excess of 190 K, as has been repeatedly done in the past (Haynes et al, 1992). For HCl-doped ice $\Delta H_{subl} = 11.2 \pm 2.8$ and for HBr-doped ice $\Delta H_{subl} = 11.7 \pm 2.8$ kcal mol^{-1}, the latter of which is in good agreement with Hudson et al., 2001. ΔH_{subl} is independent of the presence of HX in the given concentration range and equal to ΔH_{subl}(pure ice) within experimental uncertainty in agreement with the H_2O vapor pressure being that of ice even for the HX-doped ice samples in the given concentration range. However, a small counterintuitive decrease of E_{ev} may be noted in the sequence pure ice>HCl/ice>HBr/ice which is offset by a preexponential factor whose trend counteracts that of E_{ev}. The constant value of ΔH_{subl} is consistent with the fact that the vapor pressure of H_2O is independent of the amount of adsorbed HX in the range of 10^{13} to 10^{15} molecules deposited on a 0.78 cm^2 ice film. These conditions lead to low concentrations of [HX] in our experiments with an upper limit for $\chi_{HCl} = 1.2 \cdot 10^{-2}$ which is valid in the case of an ice sample a few tens of nanometers thick corresponding to point **E** of the interferogram and displayed in Fig. 4.

The unexpected stability of the vapor pressure of H_2O above the ice film in the presence of HCl follows the observation made in previous experiments concerning the prolongation of the lifetime of ice particles due to a NAT-coating (Biermann et al., 1998) in which no change of the H_2O vapor pressure was observed. However, Biermann et al. report the observation of the net rate of evaporation of pure ice and NAT/ice films and conclude that both rates are identical within experimental error which differs from our conclusions on R_{ev} and k_{cond} on pure, HCl- and HBr-doped ice. Their work also leads to H_2O mass accommodation coefficients that are in the range 0.025 to 0.05 which is at least an order of magnitude smaller than recent measurements on ice, including our work (Chaix et al. 1998; Flückiger et al., 2003). Most likely transport limitations of H_2O owing to the used high total pressure corresponding to a mbar or so led to these results at variance with all other experiments to date.

In our work, the decrease of the pre-exponential factor of the rate of evaporation of water from ice by 2 and 3 orders of magnitude for HCl and HBr, respectively, is consistent with previous results found in the literature (Hudson et al., 2001) and represents the most significant effect of HX on the H_2O evaporation from ice and thus on the lifetime of atmospheric ice particles. The observation of the negative temperature dependence of k_{cond} implies the presence of a surface-bound precursor for adsorption, hence a complex adsorption/desorption mechanism as has been discussed in the literature (Chaix et al., 1998; Flückiger et al., 2003). The decrease of both R_{ev} and k_{cond} in the presence of HX therefore may imply a modification of the ice surface at atmospherically relevant conditions. Indeed, cases (b) and (c) of Table 4 lead to an average mole fraction of HCl in a 1μm thick ice film of $\chi_{HCl} = 2$ to $4 \cdot 10^{-5}$ for $5 \cdot 10^{13}$ to $1 \cdot 10^{14}$ adsorbed HCl molecules. These concentrations represent lower limits and may be higher by at most a factor of four if one allows for the evaporation of 50 and 75% of the pure ice in the sample that is not affected by the presence of HCl as displayed in Table 3 for the amorphous and crystalline HCl hydrate, respectively.

In most cases the modification of the ice is observable by FTIR spectroscopy as displayed in Figs. 10 and 11 and clearly shows the importance of the deposition conditions, even for atmospheric conditions according to the results displayed in Table 4. Type II polar stratospheric (ice) clouds have been found on occasion in stratospheric air much warmer than the ice frost point T_{ice} (Deshler et al., 1994). A particularly pertinent observation has been made by Deshler et al. from a balloon-borne sounding of arctic stratospheric air when large ice particles with radii in the range 1–5 μm have been observed surviving for hours at temperatures several degrees (3-10) above T_{ice}. These observations and others (Goodman et al., 1997) have led to the hypothesis that a NAT coating around the ice particle prevented rapid evaporation of ice that would occur on the time scale of a few minutes in the absence of the NAT coating. In light of the present results it may be asked whether the existence of a crystalline NAT coating may be required for the decrease of the evaporation rate of H_2O or if simply the presence of adsorbed HNO_3, perhaps as amorphous HNO_3/H_2O mixture (Zondlo et al., 2000) may already be a sufficient requirement. This hypothesis begs the question as to the mole fraction or absolute concentration of HNO_3 required to lead to an effective decrease of the net evaporation rate.

The results displayed in Fig. 5 that are expressed in the Arrhenius expressions given above for the net rate of H_2O evaporation from pure ice and ice contaminated by adsorbed HX amount to a decrease of R_{ev} and k_{cond} by a factor of 5 to 6 and 15 for HCl and HBr adsorption in the indicated concentration and temperature range, respectively. These results have been obtained under conditions of molecular flow in the interest of separating the individual rates of equilibrium (3) and correspond to a relative humidity rh of a fraction of a percent. However, owing to the fact that the measured equilibrium vapor pressure of H_2O does not change upon adsorption of HX the relative decrease in R_{ev} and k_{cond} is independent of relative humidity rh because the net rate of evaporation $\Delta R_N = k_{cond}[H_2O]$ (rh-1) is a linear function of rh and affects the net rate of evaporation of pure ice and ice contaminated with HX to the same extent. Therefore, the ratio r of the net rate of H_2O evaporation from pure ice compared to HX doped ice given in Eq. (5) and the relative decrease f of the net rate of

H_2O evaporation upon doping of ice with HX displayed in Eq. (6) are independent of the relative humidity rh.

$$r = k_{\text{cond}}^{HX}/k_{\text{cond}} = R_{ev}^{HX}/R_{ev} \quad (5)$$

$$f = (k_{\text{cond}}^{HX} - k_{\text{cond}})/k_{\text{cond}} = (R_{ev}^{HX} - R_{ev})/R_{ev} \quad (6)$$

where the symbols with the superscripts correspond to the kinetic constants pertaining to HX doped ice samples.

The significant effect of HX deposition on R_{ev} from ice may also be seen in HeNe interferograms shown in Fig. 4 and summarized in Table 3, and has been observed in two other studies of the condensed phase, one for HBr (Hudson et al., 2001), the other for HCl (Krieger et al., 2002). Our values for HBr are consistent with those in the literature (Hudson et al., 2001) and may lead to a surprising increase of the lifetime for an ice particle. For HCl, Krieger et al. report a decrease of the net rate of evaporation of H_2O from ice of only 30%, whereas we observe a decrease of a factor of 2 to 15 depending on the structure of the HCl/ice surface according to Table 3. The increase of the lifetime of a 1μm thick ice film in the presence of HX may be extrapolated to the case of Cirrus clouds. As Cirrus cloud particles are large they may be approximated by bulk substrates so that the results obtained in this study may be transferable to the case of PSC's type II such that HX-doped ice particles should have an increased lifetime in the presence of HX depending on the amount of HCl adsorbed. They should thus be more available for heterogeneous reactions and so be more effective in ozone depletion processes as discussed in Solomon et al., 1997. The importance of the decrease of the net rate of evaporation of atmospheric ice particles will depend on the dose of adsorbed HX which in turn depends on the length of exposure to air masses containing HX. The HCl concentration amounts to approximately 10% of that for HNO_3 as a lower limit based on the inorganic halogen budget compared to an absolute HNO_3 concentration of roughly 10 ppb. The atmospheric HBr concentration is significantly smaller, probably on the order of a few ppt. The present work clearly shows that already a monolayer or two of adsorbed HCl may significantly slow down the H_2O evaporation rate of ice over a large volume corresponding to a layer thickness of 250 nm or more. It suggests that stoichiometric formation of crystalline hydrates such as NAT or NAM requiring large amounts of HNO_3 may not be necessary in the case of HX molecules adsorbed on ice. For HBr the smaller atmospheric abundance may be offset by the larger effect on the H_2O evaporation rate as far as lifetimes of HBr-contaminated ice particles are concerned.

Annex A: The partial pressure of H_2O over ice measured in a chamber at ambient temperature and under molecular flow conditions

A) The partial pressure of H_2O over ice, P_{H2O}, at typically 200K measured in a vessel of the same temperature T is identical to the equilibrium vapor pressure P_{eq}. In such a system the one temperature of the condensed phase as well as the chamber walls control P_{eq}. The corresponding H_2O concentration, $[H_2O]$, is equal to the molecular density given by equations (7) and (8) when either the rate (R_{ev}) or the flux (J_{ev}) of condensation and evaporation of H_2O in the presence of ice, respectively, are expressed in terms of true chemical equilibrium between the H_2O gas and condensed phase, namely

$$H_2O(g) \underset{R_{ev}}{\overset{k_{\text{cond}}}{\rightleftharpoons}} H_2O(c).$$

$$R_{\text{ev}} = \gamma\omega[H_2O] \quad \text{with} \quad \omega = \langle c(T)\rangle \frac{A_s}{4V} \quad (7)$$

$$J_{\text{ev}} = \gamma \frac{\langle c(T)\rangle}{4}[H_2O] \quad \text{with} \quad R_{\text{ev}} = J_{\text{ev}} \frac{A_s}{V} \quad (8)$$

In Eqs. (7) and (8) γ, ω, $\langle c(T)\rangle$, A_s and V are the uptake coefficient, the gas-surface collision frequency, the mean molecular velocity, the geometrical area of the substrate and the volume of the reaction system, respectively.

B) In practice, however, P_{H_2O} and $[H_2O]$ are measured in an experimental system where the condensed phase is at low temperature and whose walls are at ambient temperature. In this case the condensed phase at low temperature (T_L) and the chamber walls at ambient temperature (T_H) both control P_{H_2O} and $[H_2O]$, both of which do not correspond to the equilibrium vapor pressure P_{eq} and the equilibrium H_2O concentration, $[H_2O]$, respectively. The former situation A) corresponds to true equilibrium between the cold target and the cold chamber walls without ambiguity, except that this is a hypothetical situation rarely encountered in performed experiments. Conversely, the often encountered situation B) implies that collisions of gas at ambient temperature T_H (hot gas) occur with a target (ice) at T_L in which case P_{H_2O} and $[H_2O]$ are given by two temperatures T_H and T_L. The measured partial pressure of H_2O, P_{meas}, and the measured concentration of H_2O, $[H_2O]_{meas}$, may be calculated by postulating that the equilibrium conditions given in Eqs. (9) and (10) hold thus implying no net growth or loss of the quantity of the condensed phase at T_L.

$$J_{\text{ev}} = \gamma \frac{\langle c(T_L)\rangle}{4}[H_2O] = \gamma \frac{\langle c(T_H)\rangle}{4}[H_2O]_{\text{meas}} \quad (9)$$

$$J_{\text{ev}} = \gamma \frac{\langle c(T_L)\rangle}{4} \frac{P_{\text{eq}}}{RT_L} = \gamma \frac{\langle c(T_H)\rangle}{4} \frac{P_{\text{meas}}}{RT_H} \quad (10)$$

This means that the constraint of no net change of the quantity of the condensed phase adjusts the measured values of P_{H_2O} and $[H_2O]$ according to Eqs. (11) and (12) corresponding to an apparent equilibrium measured under realistic experimental conditions of steady state.

$$[H_2O]_{\text{meas}} = [H_2O]\left(\frac{T_L}{T_H}\right)^{1/2} \quad (11)$$

$$P_{\mathrm{meas}} = P_{\mathrm{eq}} \left(\frac{T_{\mathrm{H}}}{T_{\mathrm{L}}} \right)^{1/2} \quad (12)$$

Equations (11) and (12) show that both T_L and T_H control the measured experimental quantities P_{meas} and $[H_2O]_{meas}$. Equations (7) and (8) imply that for $T_L < T_H$, $[H_2O]_{meas} < [H_2O]$, the equilibrium concentration of H_2O at T_L, and $P_{meas} > P_{eq}$, the true equilibrium vapor pressure at T_L. In the hypothetical case that the rate constant for H_2O condensation, $(\gamma)(\omega)$, were independent of temperature, $[H_2O]_{meas} = [H_2O]$ and $P_{meas} = P_{eq} \bullet (T_H/T_L)$ would result as expected.

Acknowledgements. Generous support of this research was granted by the Fonds National Suisse de la Recherche Scientifique under contract 20-65299.01 and in part by OFES under the 5*th* framework project CUTICE of the European Union under the Environnement and Climate Program.

References

Barone, S. B., Zondlo, M. A., and Tolbert, M. A.: Investigation of the heterogeneous reactivity of HCl, HBr and HI on ice surfaces, J. Phys. Chem, 103, 9717–9730, 1999.

Bergren, M. S., Schuh, D., Sceats, M. G., and Rice, S. A.: The OH stretching region infrared spectra of low density amorphous solid water and polycristalline ice Ih, J. Chem. Phys., 69, 3477–3482, 1978.

Berland, B. S., Haynes, D. R., Foster, K. L., Tolbert, M. A., Georges, S. M., and Toon, O. B.: Refractive indices of amorphous and crystalline HNO_3/H_2O films representative of polar stratospheric clouds, J. Phys. Chem., 98, 4358–4364, 1994.

Berland, B. S., Brown, D. E., Tolbert, M. A., and George, S. M.: Refractive index and density of vapor-deposited ice, Geophys. Res. Lett., 24, 3493–3496, 1995.

Biermann, U. M., Crowley, J. N., Huthwelker, T., Moortgat, G. K., Crutzen, P. J., and Peter, Th.: FTIR studies of the lifetime prolongation of stratospheric ice particles due to NAT coating, Geophys. Res. Lett., 25, 3939–3942, 1998.

Borrmann, S., Solomon, S., Dye, J. E., and Luo, B.: The potential of cirrus clouds for heterogeneous chlorine activation, Geophys. Res. Lett., 23, 2133–2136, 1996.

Brown, D. E., George, S. M., Huang, C., Wong, E. K. L., Rider, K. B., Scott Smith, R., and Kay, B. D.: H_2O condensation coefficient and refractive index for vapor-deposited ice from molecular beam and optical interference measurements, J. Phys. Chem., 100, 4988–4995, 1996.

Chaix, L., van den Bergh, H., and Rossi, M. J.: Real-time kinetic measurements of the condensation and evaporation of D_2O molecules on ice at 140K<T<220 K, J. Phys. Chem. A, 102, 10 300–10 309, 1998.

Delzeit, L., Rowland, B., and Devlin, J. P.: Infrared spectra of HCl complexed/ionized in amorphous hydrates and at ice surfaces in the 15–90 K range, J. Phys. Chem., 97, 10 312–10 318, 1993.

Deshler, T., Peter, Th., Müller, R., and Crutzen, P. J.: The lifetime of leewave-induced ice particles in the Arctic stratosphere: I. Ballonborne observations, Geophys. Res. Lett., 21, 1327–1330, 1994.

Diehl, K., Mitra, S. K., and Pruppacher, H. R.: A laboratory study on the uptake of HCl, HNO_3 and SO_2 gas by ice crystals and the effect of these gases on the evaporation rate of the crystals, Atm. Res., 47/48, 235–244, 1998.

Dominé, F. and Xueref, I.: Evaluation of depth profiling using laser resonant desorption as a method to measure diffusion coefficients in ice, Anal. Chem., 73, 4348–4353, 2001.

Fluckiger, B. and Rossi, M. J.: Common precursor mechanism for the heterogeneous reaction of D_2O, HCl, HBr and HOBr with water ice in the range 170–230 K: mass accomodation coefficients on ice, J. Phys. Chem. A, 106, 4103–4115, 2003.

Fraser, H. J., Collings, M. P., McCoustra, M. R. S., and Williams, D. A.: Thermal desorption of water ice in the interstellar medium, Mon. Not. Astron. Soc., 327,, 1165–1172, 2001.

Gertner, B. J. and Hynes, J. T.: Molecular dynamics simulation of hydrochloric acid ionization at the surface of stratospheric ice, Science, 271, 1563–1565, 1996.

Goodman, J., Verma, R., Pueschel, R. F., Hamill, P., Ferry, G. V., and Webster, D.: New evidence on size and composition of polar stratospheric cloud particles, Geophys. Res. Lett., 24, 615–618, 1997.

Haynes, D. R., Tro, N. J., and George, S. M.: Condensation and evaporation of H_2O on ice surfaces, J. Phys. Chem., 96, 8502–8509, 1992.

Horn, A. B. and Sully, J.: Reaction and diffusion in heterogeneous atmospheric chemistry studied by attenuated total internal reflection IR spectroscopy, J. Chem. Soc., Faraday Trans., 93, 2741–2746, 1997.

Hudson, P. K., Foster, K. L., Tolbert, M. A., George, S. M., Carlo, S. R., and Grassian, V. H.: HBr uptake on ice: uptake coeficient, H_2O/HBr hydrate formation, and H_2O desorption kinetics, J. Phys. Chem. A, 105, 694–702, 2001.

Keyser, L. F. and Leu, M-T.: Surface areas and porosities of ices used to simulate stratospheric clouds, J. Colloid Interface Sci., 155, 137–145, 1992.

Koch, T. G., Banham, S. F., Sodeau, J. R., Horn, A. B., McCoustra, M. R. S., and Chesters, M. A.: Mechanism for the heterogeneous hydrolysis of hydrogen chloride, chlorine nitrate and dinitrogen pentoxide on water-rich atmospheric particle surfaces, J. Geophys. Res., 102, 1513–1522, 1997.

Koehler, B. G., McNeill, L. S., Middlebrook, A. M., and Tolbert, M. A.: Fourier-transform infrared studies of the interaction of HCl with model polar stratospheric cloud film, J. Geophys. Res. D, 98, 10 563–10 571, 1993.

Koehler, B. G.: Desorption kinetics of model polar stratospheric cloud films measured using Fourier transform infrared spectroscopy and temperature-programmed desorption, Int. J. Chem. Kin., 33, 295–309, 2001.

Krieger, U.K., Huthwelker, T., Daniel, C., Weers, U., Peter, T., and Lanford, W. L.: Rutherford backscattering to study the near-surface region of volatile liquids and solids, Science, 295, 1048–1050, 2002.

Kroes, G. J. and Clary, D. C.: Adsorption of HCl on ice under stratospheric conditions: a computational study, Geophys. Res. Lett., 19, 1355–1358, 1992.

Kumai, M.: Hexagonal and cubic ice at low temperatures, J. Glaciol., 7, 95–108, 1968.

Marti, J. and Mauersberger, K.: A survey and new measurements of ice vapor pressure at temperatures between 170 and 250 K, Geophys. Res. Lett., 20, 363–366, 1993.

Ritzhaupt, G. and Devlin, J. P.: Infrared spectra of nitric and hy-

drochloric acid hydrate thin film, J. Phys. Chem., 95, 90–95, 1990.

Schaff, J. E. and Roberts, J. T.: Towards an understanding of the surface chemical properties of ice: differences between the amorphous and crystalline surfaces, J. Phys Chem, 100, 14 151–14 160, 1996.

Schriver-Mazzuoli, L., Schriver, A., and Hallou, A.: IR-reflection-absorption spectra of thin water ice films between 10 and 160 K at low pressure, J. Mol. Struct., 554, 289–300, 2000.

Solomon, S., Garcia, R. R., Rowland, F. S., and Wuebbles, D. J.: On the depletion of antartic ozone, Nature, 321, 755–758, 1986.

Solomon, S., Borrmann, S., Garcia, R. R., Portmann, R., Thomason, L., Poole, L. R., Winker, D., and McCormick, M. P.: Heterogeneous chlorine chemistry in the tropopause region, J. Geophys. Res., 102, 21 411–21 429, 1997.

Svanberg, M., Pettersson, J. B. C., and Bolton, K.: Coupled QM/MM molecular simulations of HCl interacting with ice surfaces and water clusters-Evidence of rapid ionization, J. Phys. Chem. A, 104, 5787–5798, 2000.

Tolbert, M. A., Rossi, M. J., Malhotra, R., and Golden, D. M.: Reaction of chlorine nitrate with hydrogen chloride and water at antartic stratospheric temperatures, Science, 238, 1258–1260, 1987.

Uras-Aytemiz, N., Joyce, C., and Devlin, J. P.: Kinetics of ice particle conversion to the hydrates of HCl, J. Phys. Chem., 105, 10 497–10 500, 2001.

Warshawsky, M. S., Zondlo, M. A., and Tolbert, M. A.: Impact of nitric acid on ice evaporation rates, Geophys. Res. Lett., 26, 823–826, 1999.

Wennberg, P. O., Brault, J. W., Hanisco, T. F., Salawitch, R. J., and Mount, G. J.: The atmospheric column abundance of IO: Implications for stratospheric ozone, J. Geophys. Res. D, 102, 8887–8898, 1997.

Zondlo, M. A., Hudson, P. K., Prenni, A. J., and Tolbert, M. A.: Chemistry and microphysics of polar stratospheric clouds and cirrus clouds, Annu. Rev. Phys. Chem., 51, 473–499, 2000.

WMO (World Meteorological Organization): Scientific assessment of ozone depletion: 2002, Global Ozone Research and Monitoring Project – Report no. 47, 498 pp., Geneva, 2003.